Elastic and Viscoelastic Modeling of Cell Deformation in Acoustically Driven Microchannel

H. R. Aghaie, M. Saghafian[†] and D. Saeidi

Department of Mechanical Engineering, Isfahan University of Technology, Isfahan, P.O.B. 8415683111, Iran

†*Corresponding Author Email: saghafian@ iut.ac.ir*

ABSTRACT

Application of acoustic waves in cell manipulation and cell separation is very usual these days but considering that the acoustic force can cause what kind of changes in cell shape, is a question right now. Under the influence of the ultrasound field in specific circumstances, cell deformation can occur. In order to model this deformation, elastic and shell models are usually used for simulation. In the current study, we present a numerical procedure to investigate the cell deformation based on the viscoelastic model while the cell is exposed to a bulk acoustic wave. Second-order acoustic pressure in the resonance frequency of 8 MHz is applied to cell boundary as an acoustic force and cell deformation is determined by solving the fluid-solid interaction (FSI) physics. Results show that the viscoelastic model predicts the cell deformation closer to experimental data relative to the elastic deformation model. Kelvin, Maxwell and SLS models are used to approximate a viscoelastic behavior. The present study shows that the Kelvin viscoelastic model is more compatible with experimental data compared with previous elastic and other viscoelastic models. By applying the Kelvin model, the root mean square error (RMSE) is obtained about 0.064 at 980kpa pressure amplitude. The effect of stiffness on aspect ratio is also investigated and it's observed that the cell deformation decreases gradually by increasing Young's modulus. Results also show that in the cases with stiffness up to the 600 pa in Young's modulus, there's a sharp drop in cell deformation.

NOMENCLATURE

C_f	speed of sound in fluid	t	time
C	speed of sound in solid	V	acoustic velocity
E	Young's modulus	W	domain height
E_e	Young's modulus of the extra branch		
F	acoustic force	ε	strain
f	frequency	η	cell viscosity
H	domain height of rigid cylinder channel	λ	wavelength
h	distance between the particle and wall	μ	dynamic viscosity of fluid
k	wave number	ν	Poisson ratio
L	domain width	ρ	density of fluid
n	normal unit vector	ρ_p	density of cell/particle
P	total pressure	σ	stress
P_{amp}	acoustic pressure amplitude	τ	relaxation time
R	radius of cell/particle		
S	particle/cell surface		

1. INTRODUCTION

In recent years, there has been an interest in using acoustofluidic systems for mechanical manipulation of biological cells. When a standing wave is established in a fluid containing suspended particles or cells, these cells under the influence of acoustic waves are subjected to time average forces. Generally, this force can be used to control the trajectory of micro-size particles and cells and in some cases, it can cause deformation in biological cells and flexible particles.

Radiation acoustic force first considered by King (1934), who calculated the radiation force on the incompressible particle. Then, Yosioka and Kawasima (1955), extended his analysis and considered the compressibility of a particle in an inviscid fluid. Gor'Kov (1962), presented a simple solution for particles much smaller than the acoustic wavelength. Another useful investigation was about the effect of viscosity in determining acoustic radiation force. Doinikov (1996), showed that viscosity only affects the forces exerted on small particles. Muller *et al*. (2012), demonstrated that drag force from acoustic streaming isn't significant compared with acoustic radiation force for particles larger than 0.05 of the wavelength. Besides, in the case of two close particles, there is another acoustic force due to the particle interaction in the acoustic field. Recently, Mohapatra *et al*. (2018) and Saeidi *et al*. (2019) studied this phenomenon in the pressure nodal line and outside of pressure nodal line experimentally, respectively. Their results show that particle interaction force is not negligible while two or more particles are in the close proximity of each other. Another study, also shows this force between biological cells and silica particle as well, Saeidi *et al*. (2020).

On the other hand, cellular function and its dependency on mechanical properties have been studied widely. Stiffness is an important factor to determine cell behavior and it can be changed by disease or external effects (Oberti *et al*., 2007). For instance, a healthy blood cell is softer than a malaria blood cell (Li and Liu, 2008). Cell membrane stiffness is measured by some tools like atomic force microscopy and optical tweezers. In the first method, optical tweezer traps a single cell using a laser beam to generate force and finally, the cell is stretched tightly along the beam axis and by using this mechanism, the stiffness can be evaluated (Sleep *et al*., 1999). In the second method, by using the atomic force microscopy and a sharp probe, the force is applied to a single cell to estimates the stiffness (Mitri and Fellah, 2007). Force measurement of soft samples, is affected considerably by viscosity. Cell viscosity plays a key role in some cases and it can be used to consider a viscous contribution in cell deformation measurement. Hertz's model (Hertz, 1882) has already used for this problem. Zeng *et al*. (2007), demonstrated that viscosity affects the elastic response of samples and a viscoelastic model can solve this matter.

In past years, some studies have investigated the deformation of bubbles and water droplets in sound fields. Marston (1980) reported a formulation for determining droplet shape under acoustic waves. He presented a method to calculate acoustic stress on the droplet surface. Cell and particle deformation has been also presented recently. An experimental study was carried out by Mishra *et al*. (2014). They observed the swollen red blood cell deformation in the acoustic field and compared that with the numerical investigation. To achieve that, they used a finite element method to simulate an elastic cell deformation. Their acoustic device was based on the glass capillary in which cells were levitated and

deformed. The ultrasonic wave was excited by a PZT and acoustic pressure difference of the outer and inner layer of the cell caused the deformation. They presented the aspect ratio of the deformed cell in the range of acoustic pressure from 12.9 kPa to 978 kPa. Wijaya *et al*. (2016), investigated red blood cell stiffness in the acoustic field by both numerical and experimental methods. They obtained Young's modulus by considering a coupled acoustic-shell model and variation of cell volume in the sound field.

In this paper, we numerically simulate viscoelastic cell deformation and compare its results with experimental data of Mishra *et al.* (2014). Similar to their study, we have chosen a red blood cell as a biological part of the modeling. At first, we investigate cell deformation by considering an elastic model. Afterward, we develop a similar approach to a viscoelastic cell and apply an acoustic radiation force to the Kelvin, Maxwell and SLS models and compare their results with elastic model and experimental data.

2. GOVERNING EQUATIONS

2.1 Wave Equation

The first step of finding acoustic force on a cell is calculating the acoustic pressure field. A combination of perturbation theory and Navier-Stokes equation leads to find a pressure field in the fluid domain which is exerted to the cell boundary. By assuming that the fluid characteristics like pressure, density and velocity can be divided into three different terms including stationary, first-order and second-order terms, we have (Settnes and Bruus, 2012):

$$P = P_0 + P_1 + P_2 \tag{1}$$

$$\rho = \rho_0 + \rho_1 + \rho_2 \tag{2}$$

$$V = V_0 + V_1 + V_2 \tag{3}$$

In these equations, P, ρ, and V are pressure, density, and velocity of the fluid, respectively. Subscript 0 also represents the fluid characteristics in the absence of the acoustic field. By considering a sound wave, the first and second-order terms are added to equations (subscript 1 and 2, respectively). Substituting Eq. (1) into the Navier-Stokes equation and considering first-order approximation leads to Helmholtz equation for the first order acoustic pressure (Settnes and Bruus, 2012):

$$\nabla^2 P_1 = \frac{1}{C_f^2} \partial_t^2 P_1 \tag{4}$$

where C_f is the speed of the wave in fluid. Based on the harmonic wave, time-averaged of first-order acoustic terms are zero while the time-averaged of second-order acoustic terms are non-zero. For an inviscid fluid, the second-order acoustic pressure is obtained by (Settnes and Bruus, 2012):

$$\langle P_2 \rangle = \frac{1}{2\rho C^2} \langle P_1^2 \rangle - \frac{1}{2} \rho \langle V_1^2 \rangle \tag{5}$$

where $<\ >$ denotes the time average operator and P_2 is the second-order pressure. The time-averaged acoustic force has been called radiation force and that is given by:

$$F = \langle \iint_{S(t)} P_2(-n)ds \rangle \qquad (6)$$

here n is the surface normal unit vector and $S(t)$ is a moving particle surface. It is difficult to solve this integration over the particle boundary due to the surface movement and deformation (Yosioka and Kawasima, 1955). By implementing second-order acoustic pressure and using a Reynolds transport theorem in Eq. (6), acoustic radiation force is obtained over the equilibrium particle surface, $S(0)$:

$$- F = \langle \iint_{S(0)} P_2 nds \rangle + \langle \iint_{S(0)} \rho_0(n.V_1)V_1 ds \rangle \qquad (7)$$

To investigate the cell deformation, we apply acoustic radiation force to elastic and viscoelastic solid models in different acoustic fields and solve a Fluid Structure Interaction (FSI) physics by adopting a finite element in COMSOL software.

2.2 Equations of Solid Mechanic

In this study, we have investigated the cell deformation by considering the cell as an elastic and viscoelastic material. For elastic materials, the correlation between stress and strain is given by:

$$\sigma = E\varepsilon \qquad (8)$$

where σ and ε are the stress and strain, respectively. E refers to Young's modulus which represents an elasticity. By applying an external load, the elastic materials deform instantaneously and return to their original shape instantly when the load is removed. For this group of materials, the effect of time isn't significant.

On the other hand, for viscoelastic materials, the concept of time is mainly important. They also return to their original shape after the load will be removed, but the viscous component takes time to do (Radmacher, 1997). Viscoelasticity is made up of viscosity and elasticity and possess both behaviors. Generally, biological cells belong to this category of material (Vincent, 2012). Any arbitrary linear viscoelastic behavior can be modeled utilizing networks of springs and dashpots arranged in series or parallel (Kollmannsberger and Fabry, 2011). The spring constant and dashpot damping are analogous to Young's modulus and viscosity, respectively. Spring is used to take elastic solid behavior into account and dashpots are used to describe the viscous fluid behavior (Haase and Pelling, 2015). Most important viscoelastic models are explained below:

2.2.1 Kelvin Model

The simplest form of a viscoelastic model is obtained by the parallel connecting of a spring and a dashpot (Fig. 1(a)). In this method, total stress divided into two parts which are applied to spring and the dashpot while the strain magnitudes are equal. The

differential equation which is describing the Kelvin model is (Fung and Tong, 2001):

$$\sigma = E\varepsilon + \eta\,\dot{\varepsilon} \qquad (9)$$

where η is the particle viscosity and $\dot{\varepsilon} = d\varepsilon/dt$ is the strain rate. Final expression for strain is given by (Lopez-Guerra and Solares, 2014):

$$\varepsilon(t) = \frac{\sigma_0}{E}(1 - e^{-(\frac{E}{\eta})t}) \qquad (10)$$

where σ_0 is a constant stress at time equal to 0.

2.2.2 Maxwell Model

The Maxwell model involves the same elements (spring and dashpot), but they are arranged in a series way. In contrast of the Kelvin model, the Maxwell model considers equal stress to spring and dashpot while the strain is shared between them (Iversen, 2015). This model is illustrated in Fig. 1(b). Maxwell model can be described by the differential equation:

$$\eta\dot{\sigma} + E\sigma = E\eta\,\dot{\varepsilon} \qquad (11)$$

where $\dot{\sigma} = d\sigma/dt$ is the stress rate. The strain is obtained by (Machiraju et al., 2006):

$$\varepsilon(t) = \frac{\sigma_0}{E}(1 + \frac{E}{\eta}t) \qquad (12)$$

2.2.3 Standard Linear Solid Model (SLS)

SLS model is a combination of a spring and Kelvin element in series. After loading, the left-hand component (Fig.1 (c)), stretches immediately and due to the Kelvin unit, the stress transfers slowly in the second spring (Chester, 2012). The differential equation describing the SLS model is:

$$(E + E_e)\sigma + \dot{\sigma}\eta = EE_e\,\dot{\varepsilon} + E\eta\,\dot{\varepsilon} \qquad (13)$$

If we consider $\tau = \eta/E$ as a relaxation time, the strain response after time τ is given by:

$$\varepsilon(t) = \frac{\sigma_0}{E_e}e^{-(\frac{E_e}{\eta})t}(e^{-(\frac{E_e}{\eta})\tau} - 1) \qquad (14)$$

where E_e is the stiffness of extra branch (Chester, 2012).
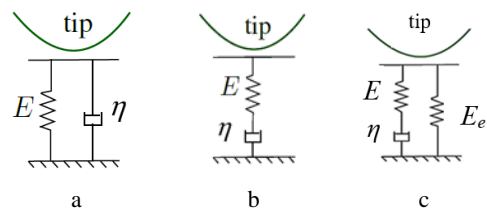
Fig. 1. Viscoelastic models base on the spring and damper connection a) Kelvin b) Maxwell c) SLS (Iversen, 2015).

3. NUMERICAL MODELING

The 2D model is implemented in a COMSOL commercial multi-physics package (version 5.2). To investigate the cell deformation in an acoustic field, we place a cell in the middle of the rectangular channel while it is exposed to an acoustic wave. The finite element method is constructed in pressure acoustic physics of COMSOL which can be used to obtain the first-order acoustic pressure distribution. Second-order acoustic pressure can be also calculated by Eq. (5) and applied to FSI physics of COMSOL, to approximate the cell deformation. 2D acoustic standing wave propagates in the rectangular domain with dimensions 1000 µm × 500 µm. A red blood cell is located in the center of the channel while the diameter of the cell is 6.2 µm. We study the cell deformation in the excitation frequency of 8 MHz while the boundary condition for the upper and the bottom walls are considered as a sound-hard wall perpendicular to wave propagation direction. The computational domain is limited by a matched boundaries in both walls in wave propagation direction and background-pressure-field generates the standing wave with $P_1 = P_{amp}\cos(kx)$. The geometry and boundary conditions are depicted in Fig. 2. Material properties, acoustic field conditions, and dimensions are given in Table 1.
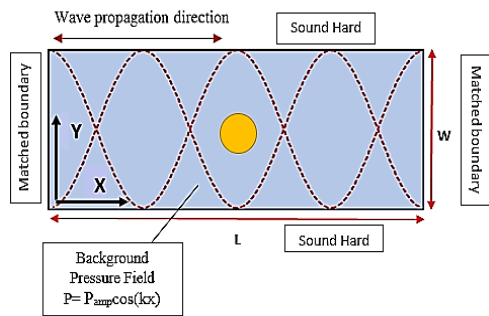
**Fig. 2. Geometry and boundary condition of the computational domain.**

Table 1 List of parameters

|	Value		Value
C	1000 (m/s)	f	8 (MHz)
E	629 (Pa)	λ	125 (µm)
v	0.499	P_{amp}	980 (kPa)
ρ_p	1139 (kg/m^3)	K	50265(1/m)
ρ	1000 (kg/m^3)	R	3.1(µm)
C_p	1680 (m/s)	L	1000 (µm)
μ	0.001 (Pa.s)	W	500 (µm)
E_e	251.6 (Pa)	τ	0.0001 (s)

3.1 Mesh Independence

The fluid domain and cell are meshed as depicted in Fig. 3(a). Mesh elements are finer close to the cell and coarser at the surrounding fluid. In the absence of an acoustic field, the cell has a circular shape and afterward, by applying the sound wave, the cell transforms into an oval shape. Cell deformation has been studied by considering the aspect ratio of the cell which is the ratio of large diameter to the small diameter of the oval. Figure 3(b), shows aspect ratio in a different number of grid elements. It's clear that for the mesh elements more than 4000, as the number of elements is increased, the aspect ratio is nearly constant. Based on that we have chosen 4210 grid elements in our study.
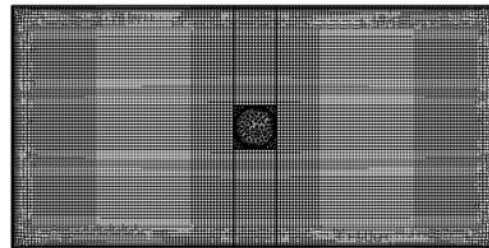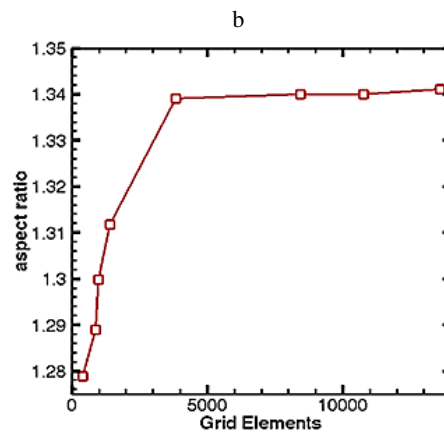

Fig. 3(a). Grid Elements of cell domain and surrounding fluid (b). Grid study for aspect ratio.
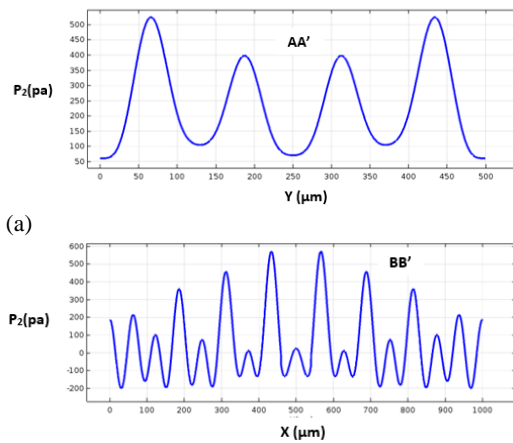
4. RESULTS

In this section, first, we discuss first and second-order pressure field and based on that we evaluate the acoustic force acting on the cell surface and finally we show cell deformation due to acoustic force and compare that with experimental data.

4.1 First and Second Order Pressure

Figure 4(a) shows the first order acoustic pressure (P_1) contour which is obtained by Helmholtz equation. Figure 4(b) is a distribution of second order acoustic pressure field (P_2) which is applied to the cell boundary. Pressure variation in x, wave propagation direction and y, perpendicular to the wave propagation direction, is also depicted in Fig. 5(a) and Fig.5 (b). As it is shown in Fig. 5(a), the pressure gradient is higher in the center of the channel, so we expect more cell deformation in this area.

(a)

(b)
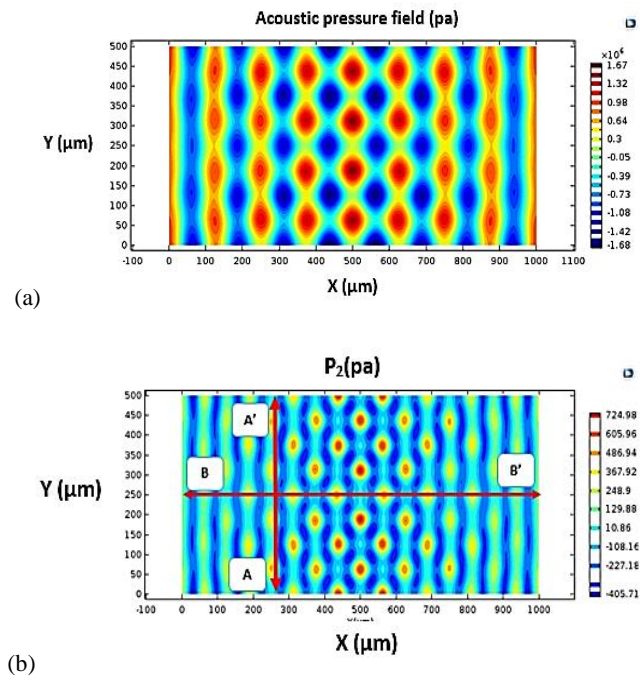
Fig. 4. First and second order acoustic pressure (a) First order acoustic pressure contour (P_1). (b) Second order acoustic pressure (P_2).


(a)

(b)

Fig. 5(a). P_2 variation in the x direction, line BB'. (b). P_2 variation in the y direction line AA'.

4.2 Force on a Rigid Cylinder

In order to verify the magnitude of the acoustic force, we compare our results with the investigation of Wang and Dual (2009). They presented a finite volume (FVM) solution to obtain an acoustic force. Table 2, shows the acoustic force on a rigid cylinder for different cylinder sizes and our results are compared with their values. Their domain is depicted in Fig. 6 and it has the same condition of Wang and Dual (2009) domain. A set of parameters is taken from their tables and readers can see details of Wang and Dual (2009). In Table 2, R and h are the particle radius and horizontal distance between the particle and wall. H and L denote the dimensions of a rectangular domain. In the worst-case scenario the force difference between Wang and Dual (2009)

modeling and presented study is about 0.8% which shows the accuracy of the current model.
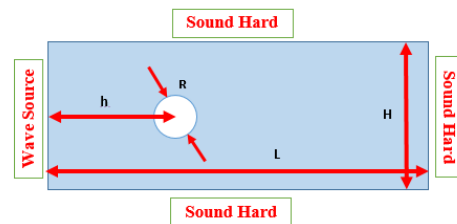
**Fig. 6. Boundary condition and dimensions of the rigid cylinder study.**

4.3 Cell Deformation

Elastic modeling: By applying the second-order acoustic pressure (P_2) to the cell surface in FSI physics of COMSOL, the equators of the cell move inward while its poles move outward in the wave propagation direction. The amount of deformation is estimated by aspect ratio. Results are compared with the experimental and theoretical study of Mishra et-- al. (2014). They investigated red blood cell deformation in pressure between 12.9 kPa-980 kPa by both experimental and numerical methods. They studied a red blood cell when it was located inside of a glass capillary tube and exposed to the high-frequency acoustic wave (Mishra *et al.*, 2014). Figure 7(a), shows their experimental setup. A red blood cell deformation is also shown in different acoustic pressure amplitude in Fig. 7(b). We compare our results with both experimental and numerical achievement of Mishra *et al.* (2014). The parameters like frequency, Young's modulus, and Poisson's ratio, are chosen the same as Mishra *et al.* (2014) study. At first, we compare the cell

Table 2 Acoustic force on a rigid cylinder (Wang and Dual, 2007)

R(μm)	L(μm)	H(μm)	h(μm)	$F_{present\ study}$(N/m)	F_{wang}(N/m)
0.715	143	14.3	53.6	7.320E-07	7.260E-07
1.43	143	14.3	53.6	3.065E-06	3.053E-06
2.86	143	28.6	53.6	1.267E-05	1.257E-05
5.72	143	28.6	53.6	6.447E-05	6.452E-05
11.44	143	71.5	53.6	2.300E-04	2.287E-04

deformation by using an elastic model with numerical and experimental data of Mishra *et al.* (2014), and results show good agreement especially in higher pressure amplitudes (Fig. 8). It can be observed that the aspect ratio increases gradually by increasing the pressure amplitude. As shown in Fig. 8, the results of the present study follow the experimental results of Mishra *et al.* (2014), better than numerical data, which is reported by them.

a

b

Pressure amplitude: 0 ➡ 980 kpa
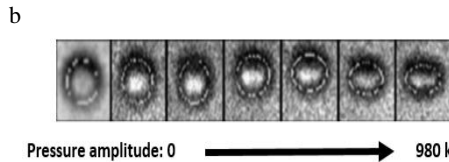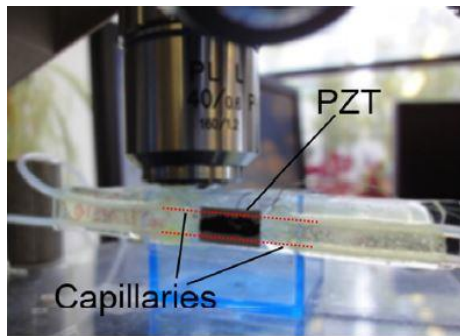
Fig. 7(a). Experimental setup of Mishra *et al.* (2014) (b). red blood cell after the deformation in acoustic field.
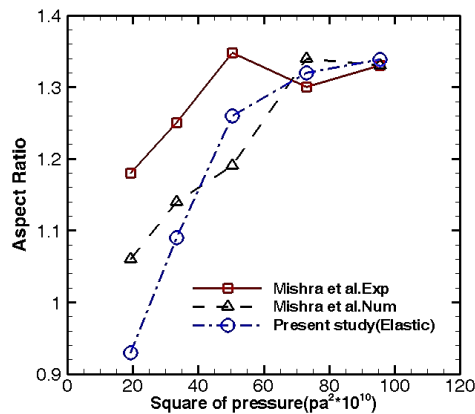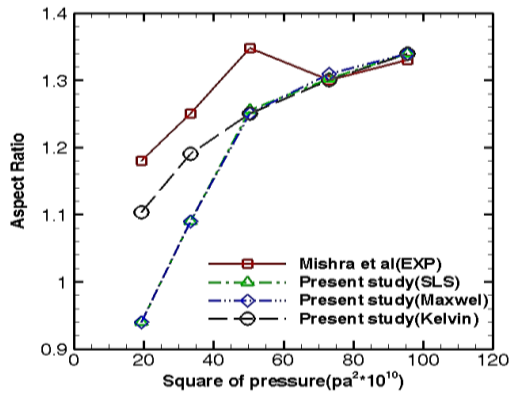

Fig. 8. Comparison of aspect ratio of elastic red blood cell in different square of pressure.

Viscoelastic modeling: Although Mishra *et al.* (2014), just considered an elastic model in their study, here we also investigate the viscoelastic model to simulate the cell deformation. Three different viscoelastic models, Kelvin, Maxwell, and SLS are considered, and their results are compared with experimental data of Mishra *et al.* (2014) in Fig. 9(a). It can be seen that Maxwell and SLS models show the same behavior while the Kelvin model has better agreement with experimental data. By considering the Kelvin model has the most accuracy, we compare that with the elastic model and experimental data in Fig. 9(b). It is clear that viscoelastic Kelvin model not only gives better agreement with experimental data in the lower square of acoustic pressure amplitudes, it is also completely matched with experimental data in high-acoustic pressure amplitudes. For better comparison, the difference between the numerical and experimental results is calculated in the Root Mean Square Error (RMSE) method. RMSE values of the Kelvin model and numerical model of Mishra *et al.* (2014) are 0.097 and 0.64 respectively. The difference percentage of the values of the present model and Mishra *et al.* (2014) are also tabulated in Table 3.

Relaxation time: Dynamic behavior of shape deformation, in particular, the relaxation time is also notable. Figure 10, illustrates the variation of aspect ratio in time transition and it's obvious, after about 1ms, there are no significant changes in deformation.

But it's not for sure because we get deformation in FSI physics and time-dependent condition, while the acoustic force is obtained by the frequency domain. Despite this inconsistency, the result is approximately acceptable. The same behavior was reported by Baskurt and Meiselman, (1996). Besides, Mishra *et al.* (2014) observed that red blood cell deformation had occurred too fast to be seen by eye.

Effect of frequency: We expect that by increasing the acoustic wave frequency, the cell deformation and aspect ratio increase as well. To investigate the effect of wave frequency on cell deformation magnitude, the range of 2-8 MHz considered in our modeling with the viscoelastic Kelvin model and our results are shown in Fig. 11. It can be observed that, as the frequency is increased, cell deformation increases. It must be noticed for frequencies less than 2 MHz, it wasn't found any remarkable deformation.

(a)
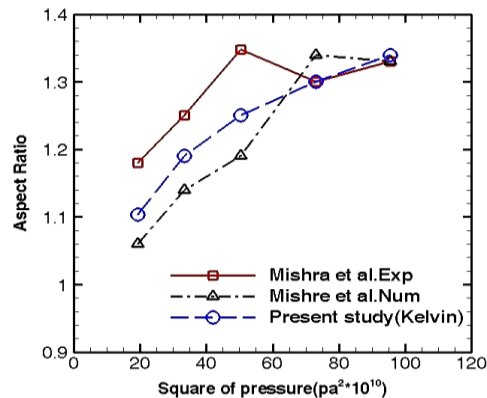
(b)

Fig. 9(a). Aspect ratio of viscoelastic models and comparison with experimental results of Mishra *et al.* (2014). (b). Comparison of Kelvin model results with experiment and numerical aspect ratios of Mishra *et al.* (2014). It's obvious that Viscoelastic Kelvin model has better agreement with experimental results in compared with Elastic model of Mishra *et al.* (2014).

Effect of cell stiffness: The mechanical stiffness of the cells, has a major influence on deformation response. There's a wide range of Young's modulus and stiffness values for biological cells (Zeng *et al.*, 2010). According to cell stiffness, the amount of the required acoustic pressure for deformation can be various. We have investigated the effect of Young's modulus on cell deformation in Fig. 12(a). In this case, the acoustic pressure amplitude and the frequency are 980 kPa and 8 MHZ, respectively. There's a sharp drop in aspect ratio to the magnitude of about 1.34 at Young's modulus 600 Pa. In the current study, the acoustic pressure amplitude and the frequency are 980 kPa and 8 MHZ, respectively. There's a sharp drop in aspect ratio to the magnitude of about 1.34 at Young's modulus 600 Pa. The stiffness of some biological cells, for instance, aortic endothelial cells or red blood cell, have been measured in this range of Young's modulus (<600 pa) (Zeng *et al.*, 2010). It's clear that for higher cell stiffness, higher pressure amplitude is needed to deform the cell. In order to investigate this issue, the aspect ratio is obtained in the normalized values of *P/E* in values from 1-2, the figure is nearly linear.
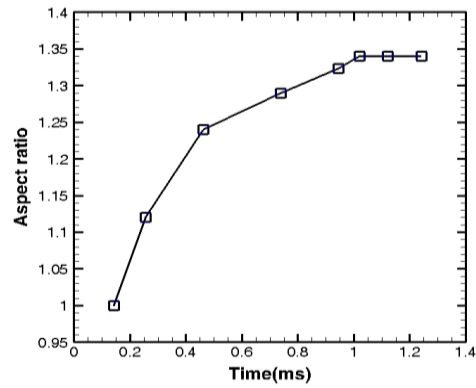
Fig. 10. Variation of aspect ratio with time.
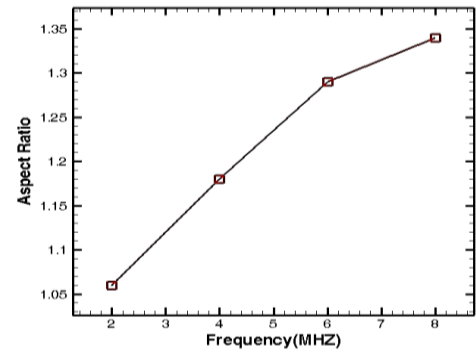
Fig. 11. Variation of aspect ratio with frequency, using viscoelastic Kelvin model.
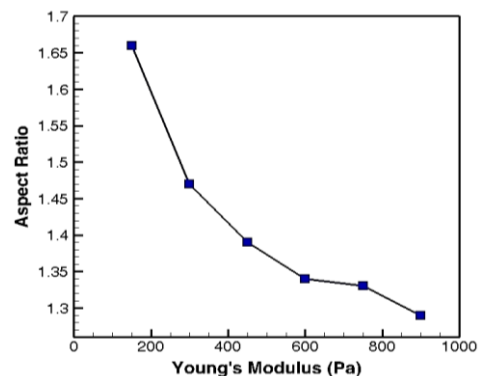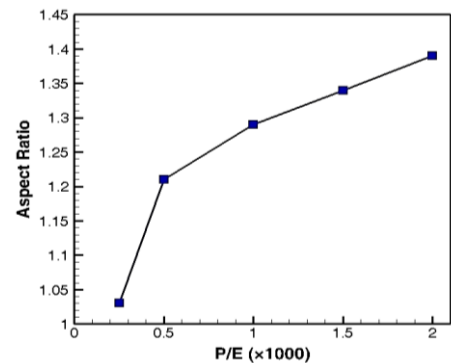
Fig. 12(a). Cell deformation variations with stiffness by applying the Kelvin model and acoustic pressure of 980Kpa. (b). Cell deformation variations with the normalized quantity (P/E× 1000).

5. CONCLUSION

In this paper, cell deformation is simulated by using a viscoelastic and elastic model while the cell is exposed to the bulk acoustic wave with a frequency of 8 MHz and an acoustic pressure amplitude of 980 kPa. Results show that the viscoelastic model predicts the cell deformation in better agreement with experimental data relative to the elastic model. In the case of the red blood cell, the Kelvin model is more accurate in a 2D model than Maxwell and SLS models. In addition, our viscoelastic simulation is quite suitable for the other case of cell deformations with different types of exciting forces. We found that by increasing the pressure amplitude, the difference between the numerical and experimental values decreases. Percentage difference and RMSE between the numerical and experimental results are obtained and it is depicted that the Kelvin model is also reliable for cell deformation problems with low acoustic pressure amplitudes. We also investigated the effect of stiffness in different aspect ratios and found that by increasing Young's modulus up to 600 Pa, the aspect ratio sharply decreases.

REFERENCES

Baskurt, O. K. and H. J. Meiselman (1996). Determination of red blood cell shape recovery time constant in a Couette system by the analysis of light reflectance and ektacytometry. *Biorheology* 33(6), 489-503.

Chester, S. A. (2012). A constitutive model for coupled fluid permeation and large viscoelastic deformation in polymeric gels. *Soft Matter,* 8 (31), 8223-8233.

Doinikov, A. A. (1996). On the radiation pressure on small spheres. *The Journal of the Acoustical Society of America* 100 (2), 1231-1233.

Fung, Y. and P. C. Tong (2001*). Computational Solid Mechanics; Advance Series in Engineering Science* Vol. 1", in. World Scientific Publishing Co. Pte. Ltd.

Gor'Kov, L. (1962).On the forces acting on a small particle in an acoustical field in an ideal fluid, in *Soviet physics - Doklady*, 773-775.

Haase, K. and A. E.Pelling (2015). Investigating cell mechanics with atomic force microscopy. *Journal of The Royal Society Interface.* 12 (104), 20140970.

Hertz, H. R. (1882). Uber die Beruhrung fester elastischer Korper und Uber die Harte. *Verhandlung des Vereins zur Beforderung des GewerbefleiBes, Berlin*, 449.

Iversen, K. (2015). *Biological Cell Models and Atomic Force Microscopy: A Literature Review*, NTNU.

King, L. V. (1934). On the acoustic radiation pressure on spheres. *Proceedings of The Royal Society A.* 147 (861),212-240.

Kollmannsberger, P. and B. Fabry (2011). Linear and nonlinear rheology of living cells. *Annual Review of Materials Research* 41, 75-97.

Li, C. and K. Liu (2008). Nanomechanical characterization of red blood cells using optical tweezers. *Journal of Materials Science: Materials in Medicine.* 19 (4), 1529-1535.

López-Guerra, E. A. and S. D. Solares (2014). Modeling viscoelasticity through spring–dashpot models in intermittent-contact atomic force microscopy. *Beilstein journal of nanotechnology* 5, 2149-2163.

Machiraju, C., A. V. Phan, A. Pearsall and S. Madanagopal (2006). Viscoelastic studies of human subscapularis tendon: Relaxation test and a Wiechert model. *Computer methods and programs in biomedicine* 83 (1), 29-33.

Marston, P. L. (1980). Shape oscillation and static deformation of drops and bubbles driven by modulated radiation stresses—Theory. *The Journal of the Acoustical Society of America* 67 (1), 15-26.

Mishra, P., M. Hill and P. Glynne-Jones (2014). Deformation of red blood cells using acoustic radiation forces", *Biomicrofluidics* 8 (3), 034109.

Mitri, F. and Z. E. A. Fellah (2007). New expressions for the radiation force function of spherical targets in stationary and quasi-stationary waves. *Archive of Applied Mechanics* 77 (1), 1-9.

Mohapatra, A. R., S. Sepehrirahnama and K. M. Lim (2018). Experimental measurement of interparticle acoustic radiation force in the Rayleigh limit. *Physical Review E* 97 (5), 053105.

Muller, P. B., R. Barnkob, M. J. H. Jensen and H. Bruus (2012). A numerical study of microparticle acoustophoresis driven by acoustic radiation forces and streaming-induced drag forces. *Lab on a Chip* 12 (22), 4617-4627.

Oberti, S., A. Neild and J. Dual (2007). Manipulation of micrometer sized particles within a micromachined fluidic device to form two-dimensional patterns using ultrasound. *The Journal of the Acoustical Society of America* 121(2), 778-785.

Radmacher, M. (1997). Measuring the el0astic properties of biological samples with the AFM", *IEEE Engineering in Medicine and Biology Magazine* 16 (2), 47-57.

Saeidi, D., M. Saghafian, S. Haghjooy Javanmard and M. Wiklund(2020). A quantitative study of the secondary acoustic radiation force on biological cells during acoustophoresis. *Micromachines* 11 (2), 152.

Saeidi, D., M. Saghafian, S. Haghjooy Javanmard, B. Hammarström and M. Wiklund (2019).

Acoustic dipole and monopole effects in solid particle interaction dynamics during acoustophoresis. *The Journal of the Acoustical Society of America* 145 (6), 3311-3319.

Settnes, M. and H. Bruus (2012). Forces acting on a small particle in an acoustical field in a viscous fluid. *Physical Review E* 85 (1), 016327.

Sleep, J., D. Wilson, R. Simmons, and W. Gratzer (1999). Elasticity of the red cell membrane and its relation to hemolytic disorders: an optical tweezers study. *Biophysical Journal* 77 (6), 3085-3095.

Vincent, J. F. (2012). *Structural biomaterials*, Princeton University Press.

Wang, J. and J. Dual (2009). Numerical simulations for the time-averaged acoustic forces acting on rigid cylinders in ideal and viscous fluids. *Journal of Physics A: Mathematical and Theoretical* 42 (28), 285502.

Wijaya, F. B., A. R. Mohapatra, S. Sepehrirahnama

and K. M. Lim (2016). Coupled acoustic-shell model for experimental study of cell stiffness under acoustophoresis. *Microfluidics and Nanofluidics* 20 (5), 69.

Yosioka, K. and Y. Kawasima (1955). Acoustic radiation pressure on a compressible sphere. *Acta Acustica united with Acustica* 5 (3), 167-173.

Zeng, D., T. Juzkiw, A. T. Read, D. W. H. Chan, M. R. Glucksberg, C. R. Ethier and M. Johnson (2010). Young's modulus of elasticity of Schlemm's canal endothelial cells. *Biomechanics and modeling in mechanobiology* 9 (1), 19-33.

Zheng, S., H. Lin, J.-Q. Liu, M. Balic, R. Datar, R. J. Cote, and Y.-C. Tai (2007). Membrane microfilter device for selective capture, electrolysis and genomic analysis of human circulating tumor cells. *Journal of Chromatography A,* 1162 (2), 154-61.